Check for updates

International Journal for Numerical Methods in Biomedical Engineering

WILEY

APPLIED RESEARCH OPEN ACCESS

A Clinically Compatible Method for Generating Preoperative Finite Element Models to Simulate Facial Appearance and Movements in Orthognathic Surgery

Marie-Charlotte Picard[1,2,3] | Mohammad Ali Nazari[1,4] | Pascal Perrier[2] | Georges Bettega[5] | Rodolphe Lartizien[5] | Michel Rochette[3] | Yohan Payan[1]

[1]Université Grenoble Alpes, CNRS, Grenoble INP, TIMC, Grenoble, France | [2]Université Grenoble Alpes, CNRS, Grenoble INP, GIPSA-lab, Grenoble, France | [3]ANSYS, Villeurbanne, France | [4]School of Mechanical Engineering, University of Tehran, Iran | [5]CH Annecy-Genevois, Annecy, France

Correspondence: Marie-Charlotte Picard (marie-charlotte.picard@univ-grenoble-alpes.fr)

Received: 3 February 2025 | **Revised:** 14 November 2025 | **Accepted:** 18 January 2026

Keywords: 3D image registration | digital twins | facial muscles | patient-specific face model

ABSTRACT

This study proposes an innovative method for generating patient-specific 3D models of the facial soft tissue, which can be integrated into clinical routine to predict the consequences of orthognathic surgery. This surgery, which impacts both facial aesthetics and functionality, requires precise tools tailored to each patient. To this end, a 3D face model has been developed, integrating anatomically precise bone structures (mandible and maxilla) and soft tissues (skin, fat, and muscles). This reference model is then fitted to each patient's anatomy using a nearly automatic method. This process requires only a manual selection of 34 landmarks to be performed in the clinical setting. The remainder of the patient-specific 3D model generation is fully automated from the patient's CT imaging data. Finally, a proof of concept is presented, featuring Finite Element simulations performed with Ansys APDL software, including orthognathic surgery and then muscle contractions applied to a patient-specific 3D model generated by the nearly automatic method.

1 | Introduction

Orthognathic surgery is a procedure designed to correct abnormal jaw positions, known as malocclusions. These anomalies can have both aesthetic and functional repercussions, influencing mastication, phonation, and breathing. Orthognathic surgeries have traditionally been planned using two-dimensional methods based on cephalometry, a technique that involves analyzing facial bone structures and soft tissues from X-rays, measuring and evaluating their proportions and spatial relationships to guide diagnosis and treatment [1–3]. However, 2D methods are no longer sufficient to accurately predict the appearance of soft tissue after surgery. As a result, much research has turned to 3D approaches [4–6], which are essential for surgical planning. These techniques play a key role in predicting optimal occlusion between upper and lower teeth.

The models most commonly used to digitally simulate this type of 3D virtual representation are the Mass-spring Model (MM) [7–9], the Mass Tensor Model (MTM) [10, 11], and the Finite Element Model (FEM) [6, 12, 13]. Mollemans et al. [10] compared these three models and concluded that the Finite Element (FE) method is the most effective, as it allows precise integration of complex, nonlinear biomechanical tissue behaviors. In return, it remains difficult to generate patient-specific FE models from their CT scans, an imaging modality commonly used in orthognathic surgery. This difficulty lies mainly in the limited visualization of soft tissues, making their extraction complex and requiring numerous manual steps. These constraints prevent the integration of such models into clinical routines. This limitation raises a critical question: how can we generate a patient-specific FE mesh that is both accurate and seamlessly adaptable into a clinical routine?

This is an open access article under the terms of the Creative Commons Attribution-NonCommercial License, which permits use, distribution and reproduction in any medium, provided the original work is properly cited and is not used for commercial purposes.

© 2026 The Author(s). *International Journal for Numerical Methods in Biomedical Engineering* published by John Wiley & Sons Ltd.

To address this question, several tools have been developed to predict the aesthetic impact of surgery while reducing the risk of complications. Examples include Maxilim, Dolphin 3D, and ProPlan CMF, as reviewed by Olivetti et al. [14–17]. However, according to Olivetti et al. [17], these 3D tools remain quite inaccurate, often less so than their 2D counterparts. Understanding the reasons for these limitations is challenging due to a lack of detailed information about how soft tissue displacements are computed or the methods used to transfer 2D predictions into 3D space. Furthermore, these tissue models lack information, particularly regarding the interior and contact areas between bony structures and soft tissues. Overall, commercial tools, such as Enlight CMF, do not provide any clear information about the internal structures of the face models and are essentially focused on the visualization of the external surface of the soft tissue. This applies also to the recent ones using deep learning approaches, such as those by Ma et al. and Du et al. [18, 19], which rely exclusively on the representation of the external surface. In addition, Hertanto et al. [20] carried out a perceptual study to assess the impact of the 3D facial predictions produced by this software after orthognathic surgery. The results revealed that 83% of the 30 patients surveyed considered that the Maxilim 3D prediction software helped reduce their anxiety and stress, and that 93% preferred to have a 3D visualization. However, 60% of participants preferred the actual final result of the surgery, highlighting the need to improve the 3D prediction software available today.

This paper presents an innovative, nearly automatic method for generating patient-specific FE models, without requiring any special skills in computer sciences or computer modeling methods on the surgeons' side, while respecting the time constraints and norms of standard clinical procedures. Once generated, these models can be used to simulate a surgical procedure (Section 4.1) tailored to the patient's specific model, as well as facial expressions resulting from facial muscle contractions (Section 4.2).

2 | Materials and Methods

For over two decades, our research team has been working on the generation of FE models specific to each patient's face. Until recently, we were able to design models that were quite accurately personalized. However, they were not directly integrable into routine clinical workflows. Our methodology is based on the manual design of a reference FE model and on the use of a nonrigid registration algorithm to morph this reference model onto the specific anatomy of each new patient. The design of the reference model is time-consuming, but it occurs only once since the same reference model is used for all the patients. The morphing phase is designed to be automatic, or with minimal manual intervention, in order to be compatible with the constraints of routine surgery planning. The advantage of a methodology that is based on FE mesh morphing is that it preserves the topology of the mesh, with a patient-specific mesh that gets the same number of nodes and elements as in the reference mesh. The Mesh-Matching (MM) algorithm, proposed by Couteau et al. [21] and applied by Chabanas et al. [22] to a human face model, deforms the external surface of the reference FE mesh to fit the patient's anatomy. This algorithm requires the segmentation of the external surface of the face tissue and of the external surface of bony structures from the patient's preoperative CT scan, which is time-consuming. Moreover, when strong local differences exist between the reference and the patient morphologies, discontinuities can occur in the geometric transformation applied to the reference mesh. This can result in distorted elements, which are not compatible with further FE simulations. In 2010, Bucki et al. [23] proposed an improvement of this algorithm, the Mesh-Match-and-Repair (MMRep) algorithm, which corrected the distorted elements by applying optimal nodal displacements. However, this method remains unsuitable for integration into clinical routine, as it still requires manual segmentation of soft tissues on patient CT scans, a particularly time-consuming step.

To address this issue, Bijar et al. [24] proposed to replace the morphing phase based on segmented surfaces with a morphing algorithm based on the whole 3D CT image. Instead of a complex and time-consuming segmentation step, the underlying idea consists of using the 3D preoperative image of the patient (CT and/or MRI) and finding the optimal nonrigid registration method that will automatically match that patient 3D image with the 3D image that was used to build the reference model. Section 2.2 describes the methodology proposed by Bijar et al. [24] and introduces the modifications of this methodology that were necessary to address the very specific case of the transformation in the context of orthognathic surgery. The reference FE model is described in Section 2.1 while the nearly automatic image-based registration method used to generate patient-specific model is explained in Section 2.2.2.

2.1 | The FE Reference Mesh

The reference FE mesh of the face has been accurately designed for a male with no irregularities in the orofacial region, referred to as the "reference subject." This facial mesh is an improved version of an earlier model of the same subject [25], originally adapted from the model developed by Nazari et al. [26]. It includes representations of the maxilla and mandible, as well as the soft tissues, which are modeled as a heterogeneous multilayer structure describing the skin (epidermis and dermis), hypodermis (Figure 1b,c), and muscles (Section 2.1.2). Stavness et al. [25] matched the original mesh to the reference CT scan. We have applied significant improvements to this model to achieve better anatomical accuracy and higher-quality elements [27]. This was done by extracting the geometry of the anatomical structures from the reference CT scan (Figure 1a) using a nearly automatic segmentation method on 3DSlicer software, then meshing these structures using Hypermesh software. Bone structures and skin are modeled by shell-type surface elements, with skin assigned a constant thickness of 1 mm. To represent the hypodermis, linear tetrahedral elements are used, integrating the muscular structures inside (see Section 2.1.2). The FE mesh generated is symmetrical with respect to the mid-sagittal plane and consists of 118,756 elements, including 106,998 tetrahedral elements for the hypodermis, 11,758 shell elements for the skin, and 25,014 nodes for the soft tissues (hypodermis and skin). Additionally, the mandible is modeled with 6114 elements and 3060 nodes, and the maxillary bone includes 6928 elements and 3631 nodes. The size of the elements was determined following a mesh sensitivity study.

20407947, 2026, 2, Downloaded from https://onlinelibrary.wiley.com/doi/10.1002/cnm.70144 by Yohan PAYAN - Cochrane France , Wiley Online Library on [05/02/2026]. See the Terms and Conditions (https://onlinelibrary.wiley.com/terms-and-conditions) on Wiley Online Library for rules of use; OA articles are governed by the applicable Creative Commons License

2.1.1 | Boundary Conditions

Realistic boundary conditions were applied to the reference FE mesh. First, the nodes at the boundary of the mesh, notably at the ears, neck and eye contour, were constrained to a zero displacement to prevent any rigid body movement in space (Figure 2a). Next, contacts between soft tissues (e.g., upper/lower lips) and between soft tissues and bones (e.g., bones/face) were defined (Figure 2b,c). Contacts can be of two types: fixed (at chin level) or sliding (for all the other contacts). The algorithm used for these surface/surface contacts is based on the Augmented Lagrangian method, which consists of an iterative series of penalty methods that tolerate small interpenetrations between structures in contact. The Augmented Lagrangian method has the advantage of guaranteeing better conditioning and is less sensitive to contact stiffness.

2.1.2 | Insertion of Muscular Structures

Integrating muscles into the reference FE mesh is an essential step both to account for the heterogeneity of the soft tissues and to predict the action of orofacial motor functions before and after surgery. As described in our previous work [27], muscle insertion into the FE mesh is performed as follows: in the tetrahedral 3D mesh of the hypodermis, a set of points is manually defined that specifies the main directions of the muscle fibers. This definition is based on data from the literature [28] and on the use of a CT scan of the reference subject, allowing for the delineation of the boundaries of muscles. These points in space represent curves that give fiber directions of each muscle and intersect mesh elements of the hypodermis. Each mesh element intersected by these curves is assigned to a specific muscle. This step is automated thanks to a code developed in Ansys APDL, which identifies the 3D elements located along the muscle curves. Each muscle element thus identified is assigned a muscle fiber direction determined from two successively positioned points of the corresponding curve. Muscles can then contract along their fiber directions. For each of these elements, an active Hill-type behavior law is used, integrated as a USERMAT law in the ANSYS APDL software by Nazari et al. [29] This law models muscle contraction oriented along a single fiber direction [29], with the future possibility of integrating two contractile fiber directions at a point [30].

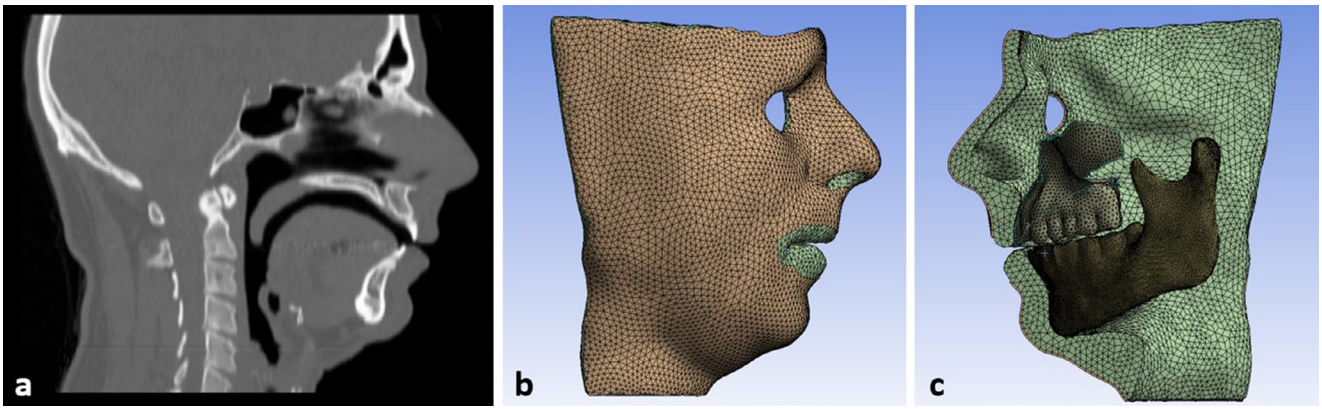

FIGURE 1 | (a) Reference CT scan. (b, c) Reference FE mesh of soft tissue (hypodermis in green, skin in orange) and bone structures, mandible and maxilla, visualized in Ansys Workbench software.

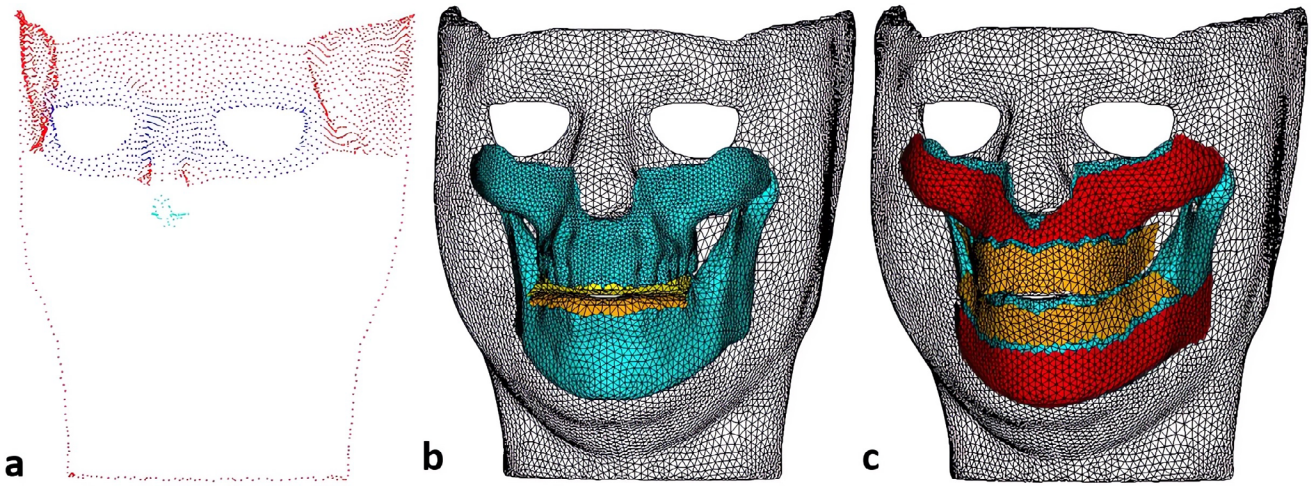

FIGURE 2 | (a) Fixed nodes in space (blue: Around the eyes, cyan: Nose and red: Around the skull). (b) Sliding contacts between the soft tissues of the lips (yellow/orange). (c) Sliding (orange) and fixed (red) contacts between bones (cyan) and soft tissue (white).

20407947, 2026, 2, Downloaded from https://onlinelibrary.wiley.com/doi/10.1002/cnm.70144 by Yohan PAYAN - Cochrane France , Wiley Online Library on [05/02/2026]. See the Terms and Conditions (https://onlinelibrary.wiley.com/terms-and-conditions) on Wiley Online Library for rules of use; OA articles are governed by the applicable Creative Commons License

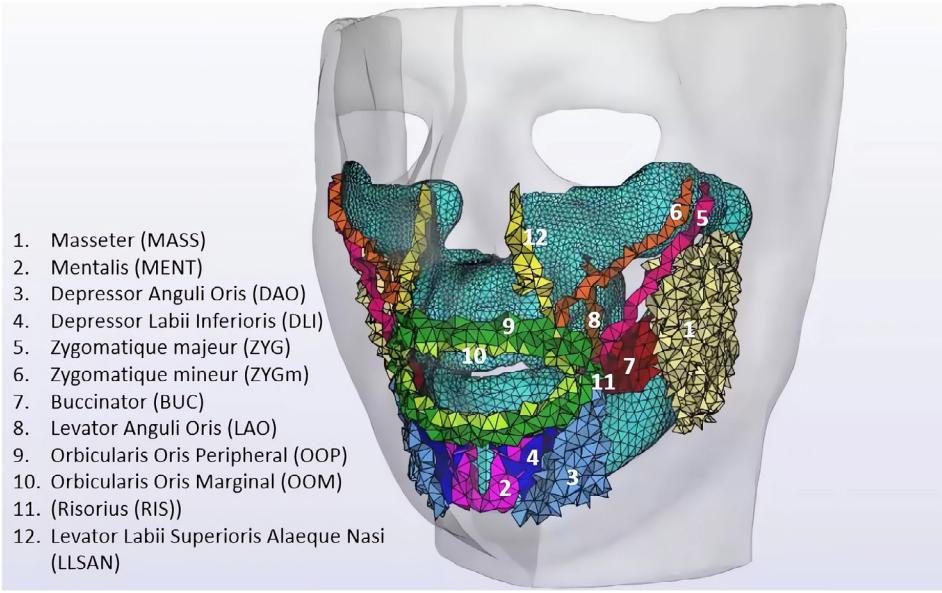

FIGURE 3 | Reference FE model with soft tissue (gray), bones (cyan), and muscles represented by tetrahedral elements (other colors).

A total of 12 muscles were integrated as tetrahedral element sets in the FE mesh: zygomaticus major and minor, orbicularis oris peripheral and marginal, levator anguli oris, buccinator, levator labii superioris alaeque nasi, risorius, depressor anguli oris, depressor labii inferioris, mentalis, and masseter (Figure 3).

2.1.3 | Material Parameters

The soft tissues of the human face are highly complex, being heterogeneous, hyperelastic, anisotropic, viscoelastic, and poroelastic. In the reference model, heterogeneity is simplified by distinguishing only the skin (epidermis and dermis) from the hypodermis. These two structures are assumed to be isotropic. They are considered hyperelastic and modeled using a second-order Yeoh law with parameters taken from Barbarino et al. [31], defined as follows:

- Hypodermis:

$$C_{10} = 400\,Pa, \quad C_{20} = 1{,}400\,Pa,$$
$$d_1 = \frac{2}{k} Pa^{-1} \quad \text{with} \quad k = \frac{2C_{10}}{1-2\nu} \quad \text{and}$$
$$\nu = 0.46, \quad d_2 = 0\,Pa^{-1}$$

- Skin:

$$C_{10} = 3{,}180\,Pa, \quad C_{20} = 14{,}500\,Pa,$$
$$d_1 = \frac{2}{k} Pa^{-1} \quad \text{with} \quad k = \frac{2C_{10}}{1-2\nu} \quad \text{and}$$
$$\nu = 0.46, \quad d_2 = 0\,Pa^{-1}$$

with C_{10} and C_{20} representing the intrinsic stiffness of the material, and d_1 and d_2 its compressibility, aiming to approximate the behavior of a nearly incompressible material.

Anisotropy is partially integrated in the hypodermis by the addition of muscles that feature a transversely hyperelastic behavior along the fiber directions (see Section 2.1.2). Viscoelasticity is modeled using Rayleigh damping, while poroelasticity is not accounted for the sake of simplicity.

2.2 | Nearly Automatic Image-Based Method for Patient-Specific Model Generation

Bijar et al.'s algorithm [24] generates patient-specific 3D models from a registration method that aligns a 3D medical image of the patient with the reference CT scan. In this study, patient identification has been anonymized to ensure confidentiality in the publication of this article. This algorithm is based on image registration applied to the entire CT volume, and it is illustrated in Figure 4. The registration is based on a two-stage approach: first a rigid/affine transformation, then a nonrigid method using FFDs (*Free-Form Deformations*). The rigid registration achieves the optimal alignment of the reference CT scan with the patient's CT scan by matching the voxels of the reference scan to those of the patient's scan, based on the intensity values of the voxels. Since an affine transformation cannot capture the local transformations required to account for geometric variations between soft tissues, an additional nonrigid transformation is necessary. This is done with the subsequent FFD transformation that deforms an object by using a three-dimensional grid, called the "control grid," made up of "control points" placed in the reference CT volume. FFD interpolates the transformation from the control points to the whole volume using B-splines. To perform these tasks, we use the *Elastix* library [32], which enables rigid and nonrigid registration of volumetric images to compute the deformation field T and the 3D displacement field, referred to as "Image-based non-rigid registration" in Figure 4. The deformation field T is computed using an optimization process, minimizing a cost function C:

$$\hat{T} = \underset{T}{\operatorname{argmin}}\, C\left(T; I_f; I_d\right), \text{with} \tag{1}$$

$$C\left(T; I_f; I_d\right) = -S\left(T; I_f; I_d\right) + \gamma \mathcal{P}(T) \tag{2}$$

20407947, 2026, 2, Downloaded from https://onlinelibrary.wiley.com/doi/10.1002/cnm.70144 by Yohan PAYAN - Cochrane France , Wiley Online Library on [05/02/2026]. See the Terms and Conditions (https://onlinelibrary.wiley.com/terms-and-conditions) on Wiley Online Library for rules of use; OA articles are governed by the applicable Creative Commons License

where T is the deformation field, I_f and I_d are the reference subject's and patient's CT scan, respectively, called "fixed" and "deformable" images. S is an intensity-based similarity measure between the two images, $\mathcal{P}$ is a penalty term, avoiding excessive element distortions that could endanger the possibility of carrying on proper FE simulations, and γ is a coefficient representing the weight of the penalty with respect to the similarity term.

Once the deformation between the two images has been calculated, the Elastix library outputs a 3D displacement field (Figure 4). This field is then applied directly to the nodes of the reference FE mesh, using Elastix's Transformix library to generate the patient-specific FE mesh (see "Application of the transformation to the nodes of the reference mesh" Figure 4).

The advantage of such a method is that it preserves the topology of the reference FE mesh. In other words, in a patient's FE mesh, only 3D coordinates of the nodes of the reference FE mesh change, while the rest remains the same:

- Labeled structures (with the corresponding identified elements) such as soft tissues (hypodermis, skin), bony structures (mandible and maxilla), and muscular elements,
- Boundary conditions, including contacts and fixed displacements, to avoid rigid body motion.

However, in the specific context of our application, this method is not applicable to the whole CT scan at once, due to several limitations. Indeed, patient CT scans often contain artifacts caused by dental appliances, common in patients requiring orthognathic surgery (Figure 5a). Strong geometric discontinuities can also appear, particularly at the level of the lips and teeth, due to too large differences in the postures of mobile anatomical structures, in addition to a lack of detail in tissue gray levels (Figure 5b,c). CT scan was chosen for its

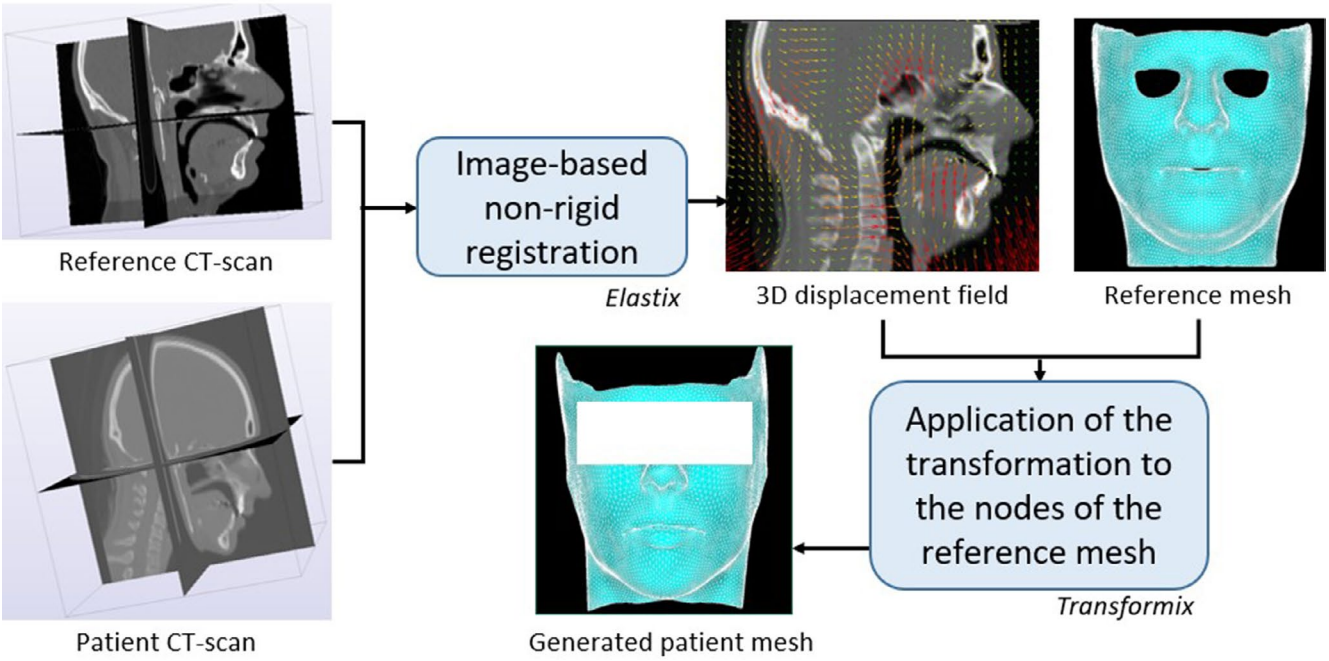

FIGURE 4 | Patient-specific mesh generation process [24].

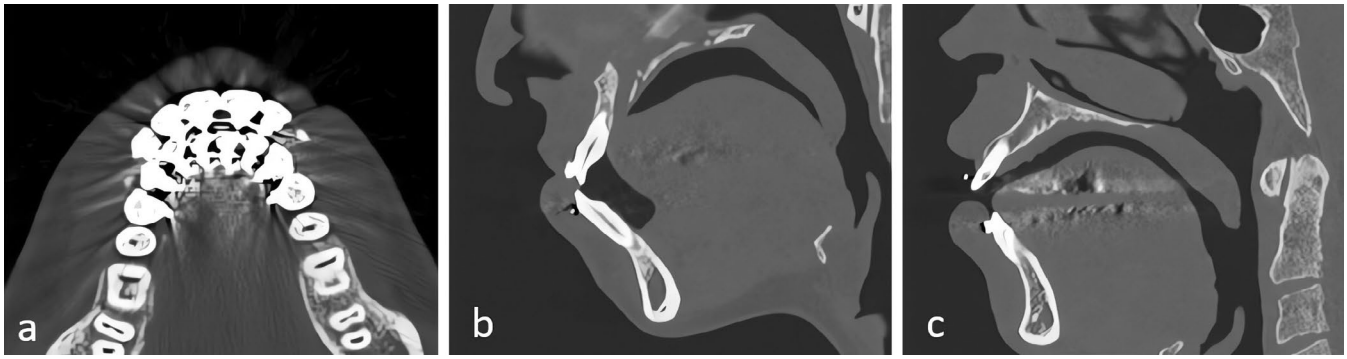

FIGURE 5 | (a) Artifacts related to the dental appliance. (b) Difficulty in differentiating gray levels on soft tissues (lips) and excessive differences with the reference CT scan in tongue position. (c) Artifacts caused by the dental appliance and significant anatomical discrepancies compared to the reference subject at the level of the lips and the upper incisors.

20407947, 2026, 2, Downloaded from https://onlinelibrary.wiley.com/doi/10.1002/cnm.70144 by Yohan PAYAN - Cochrane France , Wiley Online Library on [05/02/2026]. See the Terms and Conditions (https://onlinelibrary.wiley.com/terms-and-conditions) on Wiley Online Library for rules of use; OA articles are governed by the applicable Creative Commons License

high precision on bony structures, indispensable in orthognathic surgery, but it does not clearly visualize the fine structure of soft tissue. This limitation can cause discontinuities in patient FE meshes, rendering them unsuitable for surgical simulation.

To tackle this issue, we propose a nearly automatic three-stage method to generate 3D patient-specific models. This approach performs registrations similar to those detailed below (Section 2.2.1), based on the method of Bijar et al. [24]. Several registrations are requested, not on the entire CT scan, but specifically on regions of interest, namely the mandible, the maxilla, and the soft tissues (Section 2.2.2).

2.2.1 | Description of the Image Registration Method

To overcome the limitations caused by visibility issues on the CT scans (Figure 5), it is necessary to add anatomical landmarks in some areas in order to provide an initial spatial alignment of the volumetric images. Indeed, if the reference and the patient CT scans are too far from each other, registration may not be successful. Hence, a first rigid geometric transformation is applied to align the patient CT scan with the reference's one. This is achieved by manually placing landmarks on the bone models of both the reference subject and the patient, and by using the "*CorrespondingPointsEuclideanDistanceMetric*" provided by the Elastix library, to minimizes the Euclidean distance between the reference and the patient landmarks. This transformation requires the intervention of a clinician to locate the landmarks of the patient, the landmarks on the reference being set by us, as part of the reference data set. To make it easier for surgeons to position the landmarks, they are selected from the patient's 3D bone model (Figure 6), extracted from the patient's CT scan. This constitutes the only manual step in the entire process of generating patient-specific FE meshes and it takes about 5 min. Thirty-four landmarks were chosen for our application, positioned on identifiable points of the face, namely the nasion, the back of the skull, the most external points on the outer contours of the orbital arches, the gonions, and on the outer extremity of each tooth (×28) (Figure 6). Among them, the 28 dental markers are particularly quick to position, thanks to the clear visibility of the teeth. A module has been integrated into the CamiTK open-source software [33] to enable surgeons to position these landmarks. The advantage of this interactive module is that only those objects that are present in the patient image can be selected. For example, if the patient has some missing teeth, the corresponding reference CT scan landmarks will not be selected. In this way, a file is generated that specifies the correspondences between the anatomical landmarks in the patient's and the reference CT scans. After this rigid transformation based on the landmarks, a nonrigid transformation is applied to further refine the registration of the reference image onto the patient's image. It uses voxel intensity values of the volumetric images, as described in Bijar et al. [24]. This transformation is based on the FFD technique introduced in Section 2.2 using BSpline functions. A key parameter in this process is the size of the control point spacing σ in the grid, positioned on the reference CT scan, which can be adjusted by the user: a larger grid limits the complexity of the transformations, while a smaller grid intensifies local deformations, thus increasing the complexity of the deformations applied to the reference mesh. However, excessive transformations can generate distortions in the patient's FE mesh, compromising subsequent numerical simulations. Both the rigid and the nonrigid transformations are achieved under the constraint to minimize a cost function C formulated as follows:

$$C(\mu; I_f; I_d; P_f; P_d) = \alpha . ANC(\mu; I_f; I_d) + \beta . CPEDM(\mu; P_f; P_d) \tag{3}$$

where *ANC* (*Advanced Normalized Correlation*) denotes a correlation metric that assesses the similarity between the voxels of the fixed image I_f and those of the deformable image I_d, and *CPEDM* (*Corresponding Points Euclidean Distance Metric*) measures the Euclidean distance between two sets of corresponding anatomical points, P_f and P_d. The coefficients α and β define the weights assigned to each of these metrics in the computation of the cost. For the rigid transformation, only involving the landmark we chose $\alpha = 0$ and $\beta = 1$ and for the nonrigid transformation based on the voxels, we chose $\alpha = 1$ and $\beta = 0$.

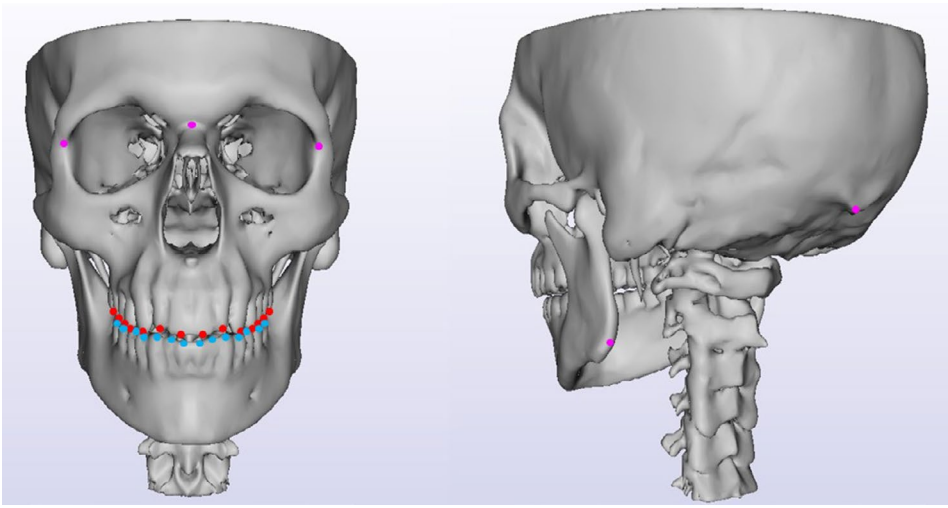

FIGURE 6 | Landmarks positioned on the reference subject, on the upper teeth (red), on the lower teeth (blue), and on the rest of the skull (pink).

20407947, 2026, 2, Downloaded from https://onlinelibrary.wiley.com/doi/10.1002/cnm.70144 by Yohan PAYAN - Cochrane France , Wiley Online Library on [05/02/2026]. See the Terms and Conditions (https://onlinelibrary.wiley.com/terms-and-conditions) on Wiley Online Library for rules of use; OA articles are governed by the applicable Creative Commons License

2.2.2 | Nearly Automatic Patient-Specific FE Mesh Generation Method

The two transformations described in Section 2.2.1 for registration are used to generate patient-specific FE meshes, but they are not applied on the whole CT scan at once, as this approach proved to be inefficient. In fact, performing registration on the entire CT scan leads to aberrant results due to the significant geometric discontinuity between the maxillary bone and the mandible. Instead, several registrations are applied successively to different regions of interest at the boundaries of bone structures and soft tissues. These areas of interest are selected by applying binary masks to the reference CT scan and using these masks as input data in the Elastix library. These masks also have the advantage of retaining only areas of interest, such as bone structures, while excluding regions affected by artifacts related to the presence of dental appliances (Figure 5). The binary masks are created by performing automatic segmentation on 3DSlicer software, based on the light intensities of the reference CT scan voxels. These masks are then spatially enlarged to better visualize the interface between bone and surrounding structures, notably soft tissue. These binary masks are introduced before computing the two transformations, rigid and FFD. It allows us to focus on the light intensities of CT scan voxels within the regions of interest, neglecting peripheral information. The advantage of this technique is that the masks are placed only once, on the reference CT scan, before the generation of any patient-specific model starts. This step is thus invisible to surgeons, as the mask does not need to be repositioned on the patient's CT scan. The global registration is therefore divided into three automatic stages: first, the generation of patient-specific bone structures, and the next two stages for the generation of facial soft tissues. The only manual step, justifying the use of the qualifying term "nearly" in "nearly automatic," involves asking the clinician to place landmarks on the patient's bone model (see Section 2.2.1, Figure 6).

The first stage consists of the generation of the FE meshes of the bony structure (mandible and maxilla). The anatomical accuracy of these models is crucial in orthognathic surgery, as the displacements applied to these bones during surgery will have a direct impact on the facial soft tissues. In this process, bone structures are geometrically deformed to match the patient's anatomy using geometric image registration presented in Section 2.2.1. Each bony structure, the mandible and the maxilla, is transformed separately, using two separate registrations applied to the CT scan regions of interest. The binary masks positioned on the reference CT scan to precisely delimit the regions of interest to be registered are displayed in Figure 8a,b.

In the 2nd stage, a mesh representing soft tissue in the patient's face is generated in two substeps. First, both the patient and reference CT images were simplified to include only two voxel categories: air (− 1000 HU and other negative values) and tissue (> 0 HU). This preprocessing step was designed to focus the registration process applied to the soft tissue on the air/tissue interface and enhance tissue contrast. Voxels corresponding to bone structures (> 300 HU) were reassigned to − 1000 HU, while those near the air/tissue boundary (between − 200 HU and 0 HU) were set to 0 HU (Figure 7a,b). This procedure standardized the air/tissue interface by eliminating the density gradient observed at this boundary and enforcing a uniform soft-tissue value (0 HU) in the transition zone. In a subsequent step, the CT image was refined by removing small components connected by pixels ("blobs") with a surface area below a predefined threshold from all 2D sagittal slices. Only regions larger than 500 pixels were retained. This filtering step effectively reduced noise within bone structures, which could otherwise be misclassified as soft tissue (Figure 7c,d). These modifications were performed automatically using a Python script.

Soft-tissue deformation was then achieved by image registration, as described in Section 2.2.1, applied to the 3D preprocessed CT images within the region of interest delimited by the mask shown in Figure 8c, which highlights the new air/tissue interface. For the nonrigid registration of the two modified images, a control point grid with a very small size is used in order to generate the 3D transformation field that will be applied to the FE mesh of the soft tissue in the reference subject. This ensures that the transformations account for local differences between the two images. As a result, the generated FE patient mesh might be highly distorted, as explained in the Section 2.2, and might include poor-quality elements that cannot be used for future numerical simulations. The goal of this stage is to accurately transform the interfaces between soft tissue and air, and between soft tissue and bones, defining the boundaries of the soft tissue. This ensures a faithful representation of the patient's anatomy and preserves bone/tissue contacts for future simulations.

Another image 3D registration, similar to that described above, is performed over the entire anatomical region to be transformed,

FIGURE 7 | Preprocessed CT scans of the reference (a) and a patient (b), where voxels with values greater than 300 HU were replaced by −1000 HU, and those between 200 HU and 0 HU were set to 0 HU. CT scans of the reference (c) and a patient (d), where blobs smaller than 500 pixels were removed in all sagittal slices.

20407947, 2026, 2, Downloaded from https://onlinelibrary.wiley.com/doi/10.1002/cnm.70144 by Yohan PAYAN - Cochrane France , Wiley Online Library on [05/02/2026]. See the Terms and Conditions (https://onlinelibrary.wiley.com/terms-and-conditions) on Wiley Online Library for rules of use; OA articles are governed by the applicable Creative Commons License

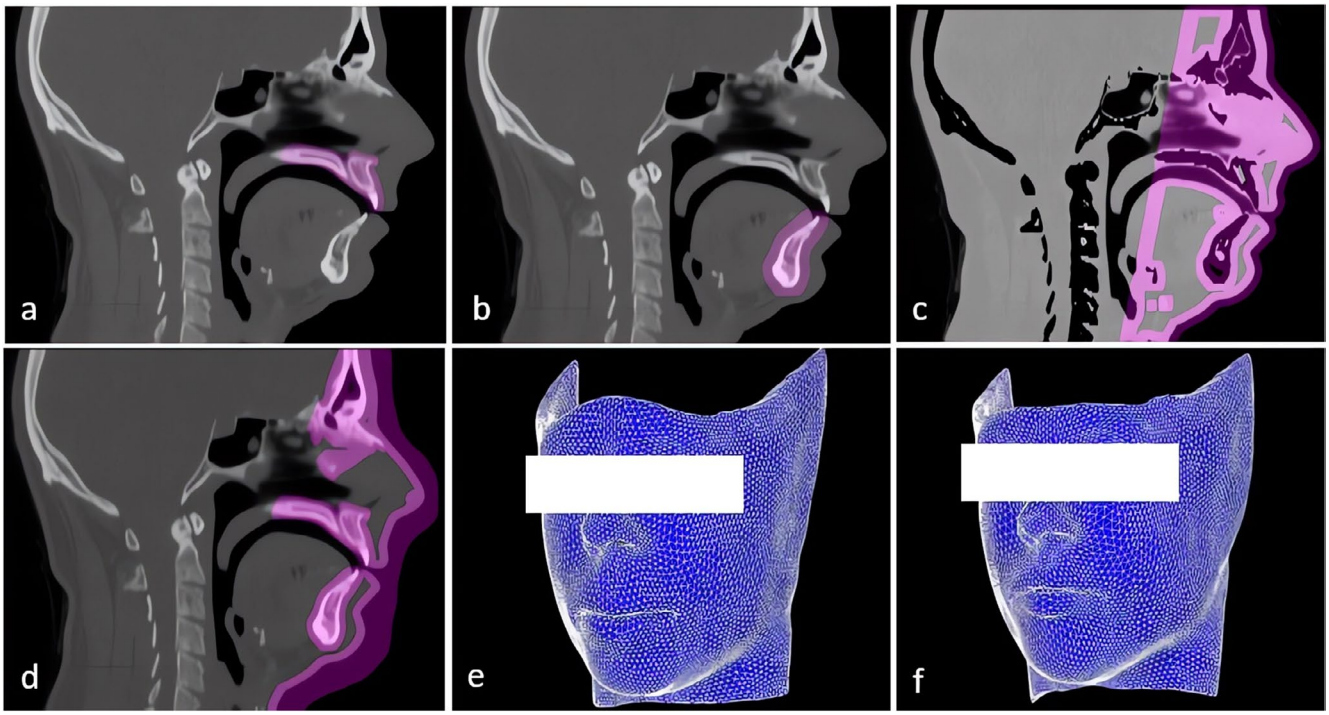

FIGURE 8 | The three stages of the proposed registration method: (1) Binary masks (pink) are placed on the reference CT scan, on the maxilla (a) and the mandible (b); (2) the masks are positioned on the outer surface of the soft tissue in the preprocessed reference CT scan (c), and an initial, "approximate" FE mesh is generated for the patient by applying a coarse geometrical transformation (large grid of control points) to the entire CT volume (d); (3) The final, accurate patient-specific FE mesh is produced by applying mechanical transformations to the approximate mesh (e) at the boundaries of the bones and the soft tissue (f).

encompassing both soft tissue and bone (Figure 8d). The control point grid size used in this registration is chosen to be large, so as to limit local deformations of the reference FE mesh. The patient mesh thus obtained is described as "approximate" (Figure 8e), since it has less anatomical accuracy; although it retains a good quality of elements, similar to that of the reference mesh.

The final stage consists of taking this "approximate" FE mesh (Figure 8e) of good element quality, and mechanically deforming it by applying an imposed displacement to all the mesh nodes on the outer surface using Ansys APDL software, in order to reposition them at the final coordinates obtained in stage 2. The result is a patient anatomy faithful to reality (Figure 8f), while preserving sufficient element quality for subsequent simulations. Fully automated FE mesh generation takes around 1 h on a computer equipped with an Intel Xeon W-2155 CPU (3.30Ghz) and 64 GB of RAM and can be started at any time according to the surgeon's preferences. Image registration alone takes around 30 min while steps (a) to (e) take around 20 min: 5 min for steps (a) and (b), 10 min for steps (c,d), and 10 min for the mechanical registration. The remaining time is devoted to positioning the muscle structures and calculating the orientation of the muscle fibers.

The evaluation of this method is presented in Section 3 and this approach was evaluated on 24 patients who underwent orthognathic surgery.

3 | Results: Evaluation of Patient-Specific Fe Meshes

An evaluation of the nearly automatic method described in Section 2.2.2 was carried out on 24 patients. Two key aspects were analyzed: the anatomical fidelity of the generated model (Sections 3.1 and 3.2) and the quality of the FE mesh (Section 3.3), to ensure its use in future FE simulations.

3.1 | Quantitative Evaluation of the Anatomical Fidelity of the Generated Meshes

To evaluate the patient-specific 3D models generated with our method, it is necessary to get the "real" external surfaces of the bones and soft tissue in each patient. These surfaces are generated from the patient's preoperative CT scan. The 3DSlicer software offers a dedicated segmentation module, enabling areas to be selected according to the gray levels of CT scan voxels, expressed in Hounsfield units. This thresholding process is used to reconstruct the 3D external surfaces of bones and soft tissue, using the marching cubes algorithm [34]. These surfaces, referred to as "real", are represented by extremely dense point clouds, with submillimeter distances between points. This accuracy enables precise calculation of deviations between generated and real anatomical structures, with these deviations being evaluated using a Euclidean distance metric.

20407947, 2026, 2, Downloaded from https://onlinelibrary.wiley.com/doi/10.1002/cnm.70144 by Yohan PAYAN - Cochrane France , Wiley Online Library on [05/02/2026]. See the Terms and Conditions (https://onlinelibrary.wiley.com/terms-and-conditions) on Wiley Online Library for rules of use; OA articles are governed by the applicable Creative Commons License

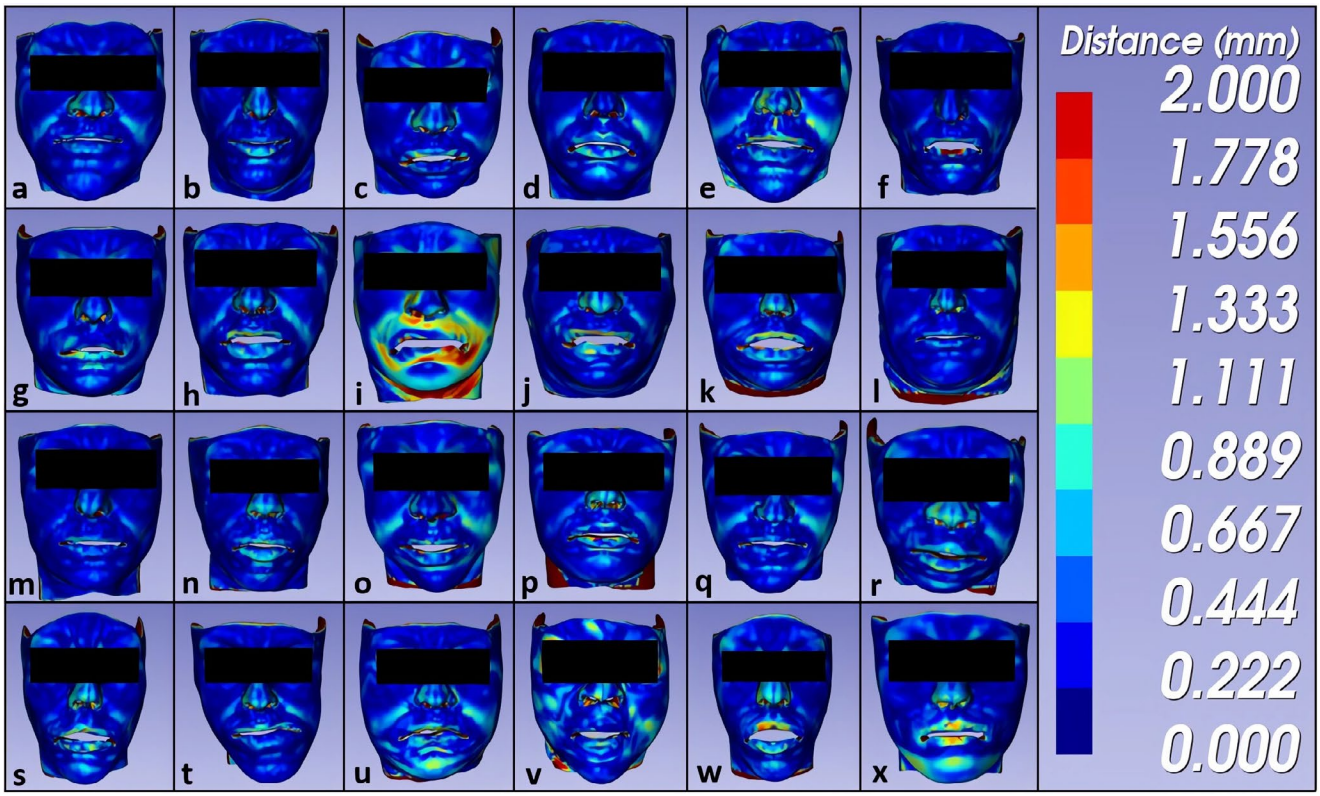

FIGURE 9 | Color map showing the Euclidean distance between the generated patient FE meshes and the corresponding real patient 3D surfaces.

The nearly automatic mesh generation method was evaluated on 24 patients based on their preoperative CT scans. These patients were selected based on the criterion that they were scheduled to undergo mandibular or maxillary orthognathic surgery, with or without genioplasty, regardless of the underlying indication (malocclusion, sleep apnea syndrome, temporomandibular joint dysfunction, etc.). Figure 9 shows maps representing the distances between the nodes of the generated patient FE meshes and the nearest points on the highly dense point clouds of the actual anatomical surfaces. For the majority of patients, errors are less than 2 mm in the most complex regions to generate due to geometric discontinuities, and less than 1 mm for the rest of the face (see Section 3.2 for the values). It should be noted that the majority of errors occur at the lips, a finding also reported in most studies in the literature, notably in the review by Olivetti et al. [17].

The model of patient i (Figure 9) could not be generated correctly due to a large number of artifacts present in the CT scan, resulting in a loss of soft-tissue visibility. Since the automatic registration method relies on tissue voxel intensities, it cannot be reliably applied in this case. Therefore, this patient was excluded from further analysis.

It is also interesting to note an error in the lower lip of patient f (Figure 9). This is also the result of artifacts on the patient's CT scan, although less pronounced than in patient i. These artifacts appear as bright streaks on the images, particularly on the sagittal slices, interrupting the continuity of the lips in certain sections. During the preprocessing of the CT scan, the step of removing blobs of less than 500 pixels on the sagittal slices incorrectly induced a partial removal of the region corresponding to the lower lip.

To analyze these results in greater detail, a statistical analysis is performed in Section 3.2.

We focus in particular on the results generated for one patient (patient n, Figure 9), which will be used in Section 4, where proofs of concept for orthognathic surgery and facial expression simulation are presented. This patient is presented in Figure 10a which shows a mapping of Euclidean distances between the real and generated patient data. These deviations are less than 2 mm. Figure 10b,c shows the same model superimposed on the patient's preoperative CT image, to visualize the accuracies of the external and internal surfaces. Indeed, an analysis of the geometry of the internal surface of soft tissue is essential for further simulations of the consequences of muscle activations on postsurgical facial appearance of the patients. Furthermore, contact conditions have been defined between bones and soft tissue and excessive gaps or interpenetration can render these contacts ineffective, making the FE meshes of patients unsuitable for future simulations.

3.2 | Statistical Analysis

In order to improve the analysis of Figure 9, a statistical study was carried out on 23 patients. Patient i was excluded from this analysis due to a significant number of artifacts present on their CT scan, making it impossible to properly visualize the soft tissues and thus generating significant errors in the corresponding 3D face model (see Section 3.1). In order to detect possible differences in the accuracy of the representation of facial soft tissues in the generated patient meshes depending on the location in the face, we considered four different anatomical regions in the face: the lips, the nose, the cheeks, and the chin. This was done in the face meshes on the

20407947, 2026, 2, Downloaded from https://onlinelibrary.wiley.com/doi/10.1002/cnm.70144 by Yohan PAYAN - Cochrane France , Wiley Online Library on [05/02/2026]. See the Terms and Conditions (https://onlinelibrary.wiley.com/terms-and-conditions) on Wiley Online Library for rules of use; OA articles are governed by the applicable Creative Commons License

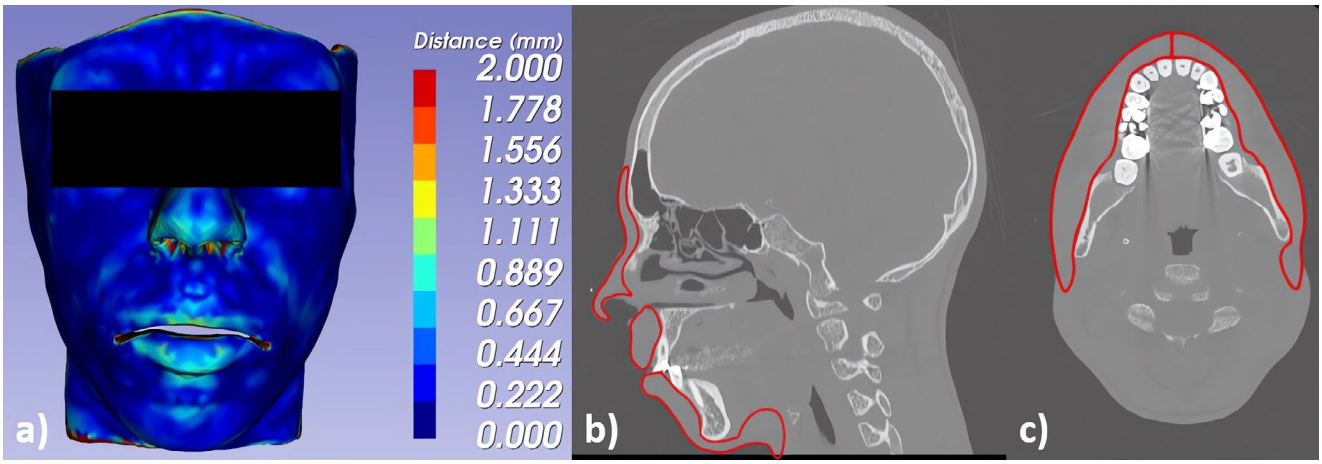

FIGURE 10 | Comparison of the generated and real faces for patient *n*: (a) Deviations (mm) between the generated patient FE mesh and the actual internal and external surfaces of the soft tissue, measured on the patient's CT scan. Visualization of the boundaries of the patient's FE mesh (in red) superimposed on his CT scan, in sagittal (b) and axial (c) views.

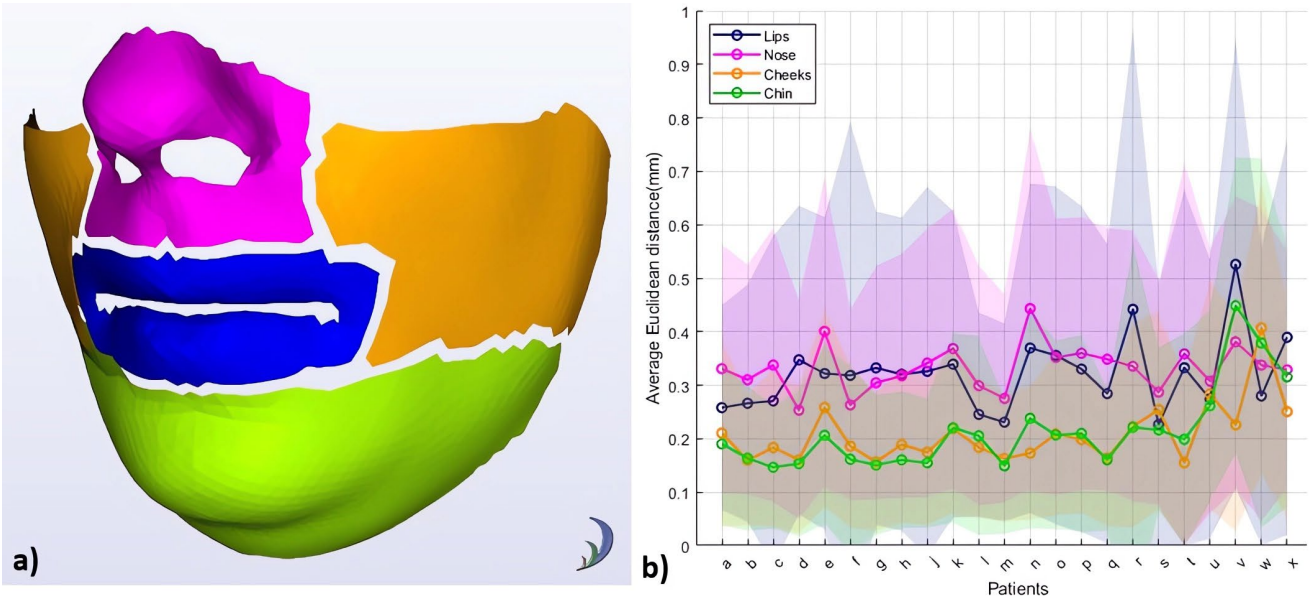

FIGURE 11 | (a) Reference model subdivided into four areas: Lips in blue, nose in pink, cheeks in orange, and chin in green. (b) Average differences (circles) and their standard deviations within each region (shaded areas correspond to + and − one standard deviation around the average) between the generated meshes and the actual surface of the face extracted from the CT scans.

basis of the node indices, which are the same in the reference mesh and in all the patient meshes. Figure 11a shows these regions on the external surface of the reference mesh. Figure 11b shows for each patient the average value of the error computed on the whole facial regions, together with the averages of the specific errors in each of the four regions of interest. Table 1 summarizes the overall averages computed across the 23 patients. The total average deviation across these areas is 0.27 mm, with respective values of 0.32 mm for the lips, 0.33 mm for the nose, 0.21 mm for the cheeks, and 0.22 mm for the chin (Table 1).

The largest errors (> 2 mm) are mainly located in the lip region, as also reported in the literature [17] and also in the nose region. The maximum error, 3.64 mm (Table 1), is observed on the lower

TABLE 1 | Means, standard deviation, and minimum and maximum values of the differences across the 4 zones for the 23 patients in mm (except for i).

Zone	Means	Standard deviation	Min	Max
Lips	0.3211	0.3035	0.00005	3.6416
Nose	0.3322	0.2441	0.00000	2.3076
Cheeks	0.2102	0.1591	0.00002	1.6339
Chin	0.2186	0.1817	0.00000	2.2919
Total	0.2687	0.2187	0.00000	3.6416

20407947, 2026, 2, Downloaded from https://onlinelibrary.wiley.com/doi/10.1002/cnm.70144 by Yohan PAYAN - Cochrane France , Wiley Online Library on [05/02/2026]. See the Terms and Conditions (https://onlinelibrary.wiley.com/terms-and-conditions) on Wiley Online Library for rules of use; OA articles are governed by the applicable Creative Commons License

lip of patient f. This error results from the second stage of CT scan preprocessing, which eliminates blobs smaller than 500 pixels. The presence of artifacts induced the removal of the lower lip, which corresponded to sections smaller than 500 pixels on sagittal slices.

A notable error of 3.40 mm is observed at the patient's lips. This value is unreliable because it results from an inadequate measurement of the distance between the generated facial mesh and the actual surface extracted from the CT scan. This inaccuracy can be explained by the fact that the lips are almost closed and that the marching cubes method only captures the external surface of the tissues without any information on the interface between the lips. The other errors in the lips area are essentially below 2 mm, which is acceptable. For the other regions, no error exceeds 2 mm between the models and the real surfaces.

3.3 | Elements' Quality of the Patient's FE Mesh Generated

When the reference FE mesh is deformed to fit the patient's morphology, there is a risk of degrading the quality of the elements, which can compromise the validity of future numerical simulations, or induce convergence issues. To evaluate mesh elements' quality, various geometric criteria are available in Ansys APDL and Ansys Workbench. We focus in particular on a global metric proposed by Ansys Workbench, called *Element Quality*, whose values range from 0 (poor quality) to 1 (excellent quality). It is calculated according to the (Formula 4), where n designates the total number of edges in the element and L_i represents the length of the i-th edge:

$$Q = \frac{\text{element_volume}}{\sqrt{\left(\sum_{i=1}^{n} L_i^2\right)^3}} \tag{4}$$

Figure 12 shows a histogram illustrating the quality of the elements in the tetrahedral meshes representing soft tissue for the 24 patients studied in Sections 3.1 and 3.2. Importantly, the reference FE mesh, constructed using a Hypermesh software optimization method to maximize element quality, displays higher quality than the patient FE meshes (Figure 12 in red). These meshes lose quality since the reference FE mesh is deformed. Nevertheless, the huge majority of elements in the patient-specific meshes have a quality larger than 0.5, making them suitable for future numerical simulations.

4 | Proof-of-Concept of Patient-Specific Fe Models for Soft Tissue Function Prediction

4.1 | Face Deformation From Orthognathic Surgery

Various software packages are now available to simulate bone cuts in orthognathic surgery on virtual 3D models. However, their main drawback lies in the fact that they operate on surface models rather than directly on the FE mesh. This approach results in a loss of the FE mesh topology, as well as the global mesh boundary conditions, for both cut parts. To avoid this,

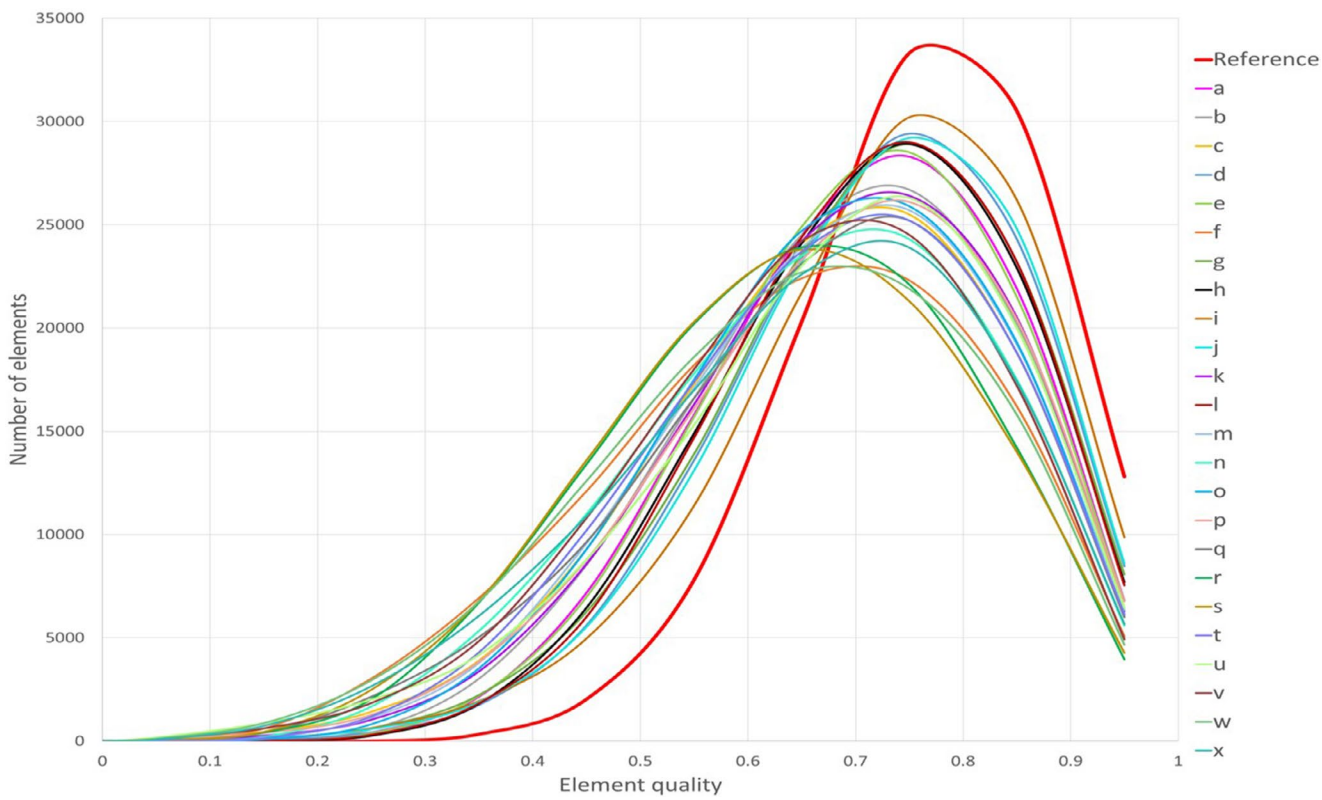

FIGURE 12 | Histogram of the *Element Quality* (Q) of tetrahedral elements in the reference soft tissue mesh and in patient-specific soft tissue meshes, evaluated on the 24 patients included in this study, according to the Ansys Workbench software quality criterion.

20407947, 2026, 2, Downloaded from https://onlinelibrary.wiley.com/doi/10.1002/cnm.70144 by Yohan PAYAN - Cochrane France , Wiley Online Library on [05/02/2026]. See the Terms and Conditions (https://onlinelibrary.wiley.com/terms-and-conditions) on Wiley Online Library for rules of use; OA articles are governed by the applicable Creative Commons License

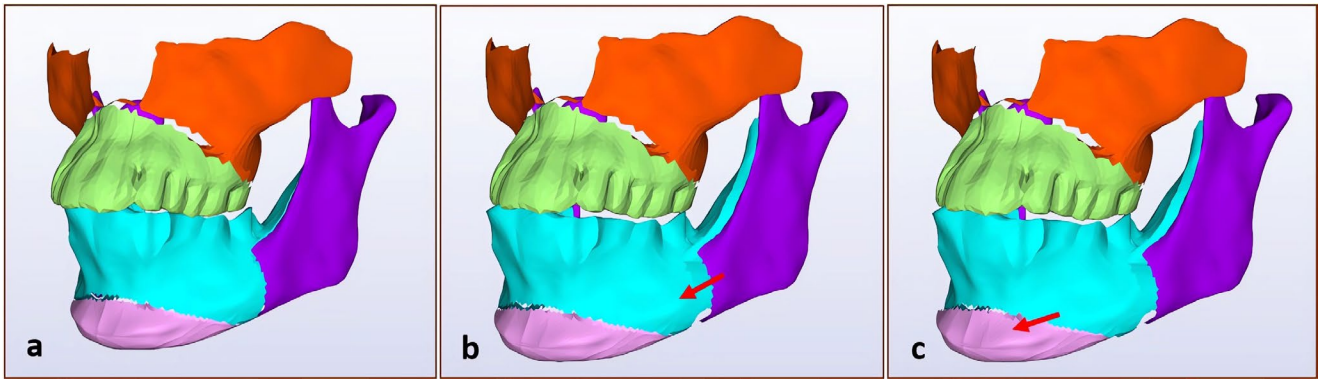

FIGURE 13 | (a) FE mesh implementing cut-out of the patient's mandible and maxilla (LeFort I osteotomy), (b) Bilateral Sagittal Split Osteotomy (BSSO) with the "Z-cut," and (c) Genioplasty with the flat cut.

we have developed a module integrated into the CamiTK open source software. This module can access a 3D FE mesh, such as that of the mandible or maxilla, and perform cuts used in various commonly used surgical techniques. It specifically implements maxillary cutting through Le Fort I osteotomy (Figure 13a in green and orange), mandibular cutting via Bilateral Sagittal Split Osteotomy (BSSO), which involves a "Z"-shaped cut of the mandibular ramus (Figure 13b in blue and purple), and genioplasty using a planar cut (Figure 13c in pink). These types of osteotomies are particularly useful for correcting Class II malocclusions, characterized by a retruded lower jaw (retrognathia), and Class III malocclusions, where the lower jaw is excessively protruded (prognathism). A particular feature of this module is that it preserves the topology of the patient's FE mesh, retaining all node indices and elements required for boundary conditions such as contacts. The user can thus apply rotation and/or translation of bone structures along the three main axes. A file is automatically generated to record the displacements of three points on the transformed 3D model. This approach avoids the direct application of rotations during numerical simulations, considering only displacements in order to speed up the calculation.

As an illustration, orthognathic surgery was simulated on the patient *n* shown in Figure 10. This patient underwent mandibular surgery consisting of a BSSO, a technique for advancing the mandible by cutting the mandibular branches (Figure 13b), and a genioplasty (Figure 13c).

To avoid the complexity of handling elements cut by the numerical surgical technique, and the necessity to generate new elements from those cut, the mandible mesh was refined with millimeter-sized elements. This size corresponds to the thickness of the saw used during surgery, and results in a mesh comprising 23,469 nodes and 46,732 elements. Therefore, the core idea is to remove all elements that intersect the saw cuts. Increasing the number of elements in bone structures has a minimal impact on numerical simulation time, as the bones, modeled as rigid bodies, are subject to restricted boundary conditions. Their displacement is controlled with three mesh points, affecting only three nodes, regardless of the total number of elements. The result of a surgical simulation on the patient *n* is shown in Figure 14 after a BSSO in (b) and a genioplasty in (c).

4.2 | Face Deformations From Muscles Activations

Patient-specific FE meshes can then be used not only to simulate bone displacements and their consequences on facial soft tissues after orthognathic surgery, but also to analyze the functional effects of muscle contractions after bone repositioning. Muscles, defined as sets of elements in the reference hypodermis FE mesh (see Section 2.1.2), are also present in the generated patient FE meshes. However, after the geometric transformation, the lines of points defining the directions of the muscle fibers in the reference mesh no longer represent the directions of the muscle fibers in the patient's mesh. This discrepancy arises because the patient's mesh underwent not only geometric transformations but also mechanical changes during the last stage of the registration method. To recalculate muscle fiber directions accounting for both the geometrical and the mechanical transformations, an automatic algorithm was developed to determine the elements that include these points in the reference FE mesh, and then deduce the position of these points in the generated patient FE mesh by interpolation calculations. A new muscle fiber direction is thus assigned to each muscle element in the patient-specific FE meshes. Thanks to our nearly automatic method, it is possible to generate the patient's FE mesh and directly simulate muscle contraction by selecting the desired muscle.

Figure 15a shows the effect of contractions of the *levator labii superioris alaeque nasi* (LLSAN) muscle on the reference FE mesh, responsible for nose elevation. Figure 15b,c shows contraction results for the same muscle (LLSAN) for patient a and *n* (Figure 9). Boundary conditions, as well as material properties, FE mesh topology, and contacts, have been kept identical in both models, and bone mesh nodes were fixed.

5 | Discussion and Conclusion

This paper presents an innovative, nearly automatic method for generating 3D patient-specific FE meshes of facial soft tissue, ready for use in numerical simulations. The ultimate goal of this work is to use this method as an initial step in a fast and reliable clinical process that takes into account speaker-specific characteristics to predict the outcome of orthognathic surgery. Subsequent steps will include simulating orthognathic surgery and predicting the aesthetic and functional consequences of

20407947, 2026, 2, Downloaded from https://onlinelibrary.wiley.com/doi/10.1002/cnm.70144 by Yohan PAYAN - Cochrane France , Wiley Online Library on [05/02/2026]. See the Terms and Conditions (https://onlinelibrary.wiley.com/terms-and-conditions) on Wiley Online Library for rules of use; OA articles are governed by the applicable Creative Commons License

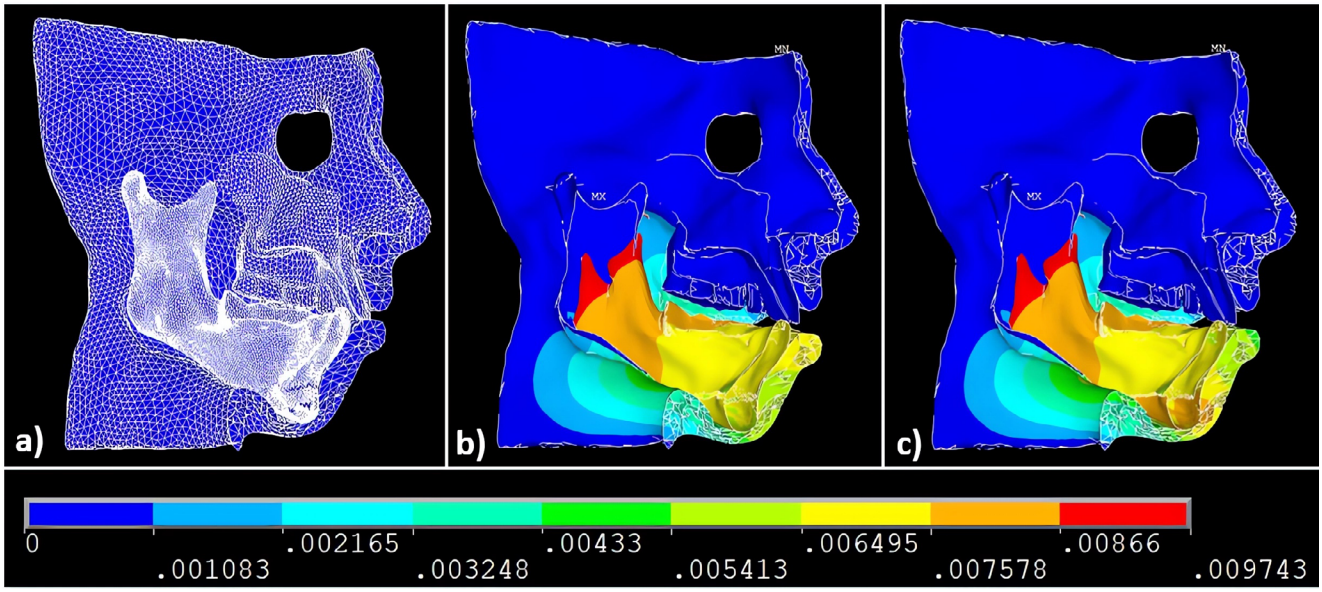

FIGURE 14 | Total nodal displacements observed in the facial soft tissues of the FE mesh of patient *n* during a simulated orthognathic surgery: (a) Patient's half-mesh preoperatively (sagittal view), (b) facial modifications after mandibular advancement (bilateral sagittal split osteotomy, BSSO) with rotation and translation, (c) facial modifications after additional genioplasty.

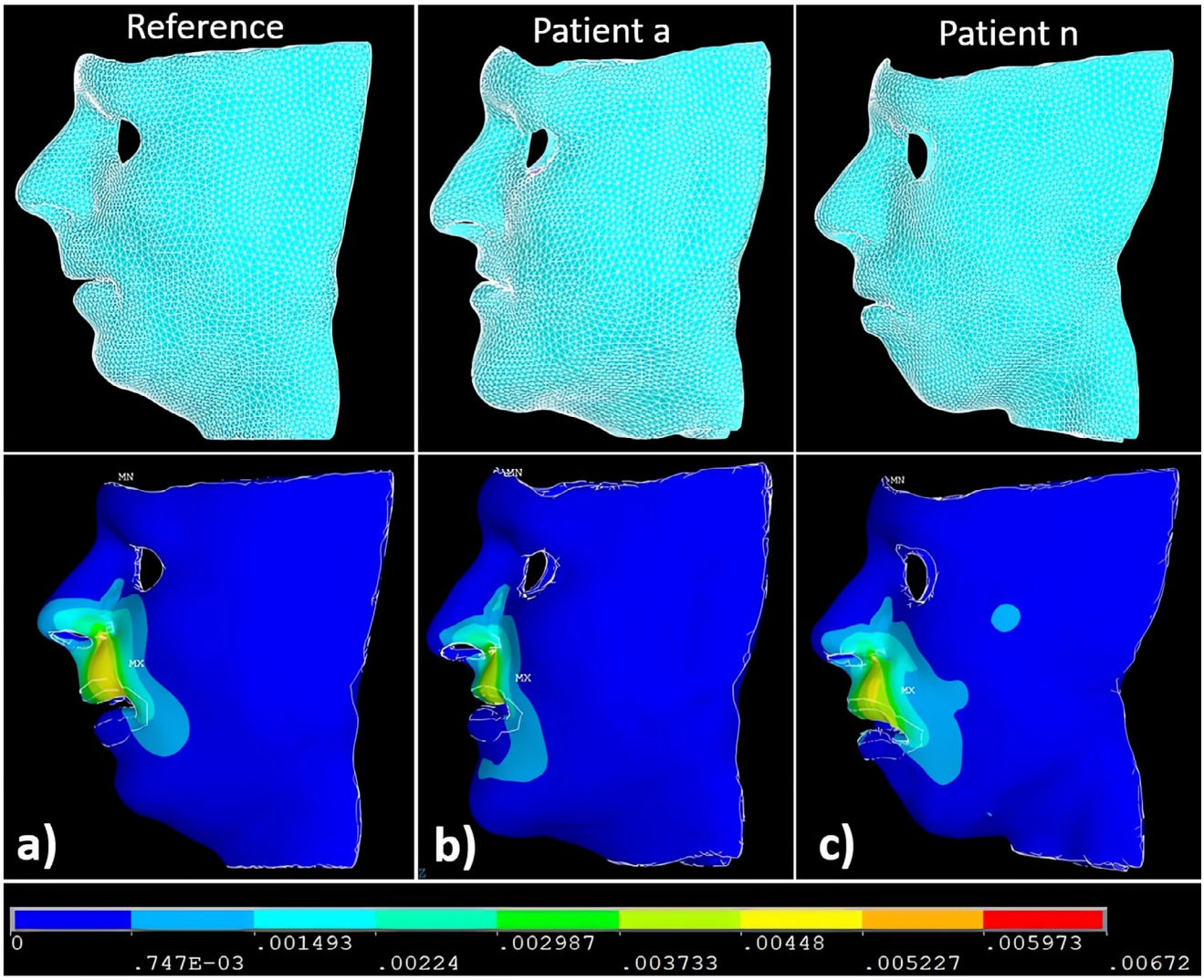

FIGURE 15 | Directional displacement (m) of reference FE mesh nodes (a), and of patients a (b) and *n* (c) induced by LLSAN muscle contraction.

20407947, 2026, 2, Downloaded from https://onlinelibrary.wiley.com/doi/10.1002/cnm.70144 by Yohan PAYAN - Cochrane France , Wiley Online Library on [05/02/2026]. See the Terms and Conditions (https://onlinelibrary.wiley.com/terms-and-conditions) on Wiley Online Library for rules of use; OA articles are governed by the applicable Creative Commons License

bone repositioning. Our approach makes this prediction possible by (1) modeling the mechanical interactions between facial soft tissues and bony structures in three dimensions, and (2) incorporating within the facial tissues muscle structures, whose bony insertions and fiber orientations are modified by skeletal restructuring. A proof of concept is provided, showing the generation of FE meshes for 24 patients, as well as simulations of facial movements induced by specific muscle contractions performed using these meshes in two different contexts.

This nearly automated process integrates the creation of 3D models of bones (surface) and soft tissue (volume), including skin (epidermis and dermis) and hypodermis with passive tissues and muscles. It also includes meshing, defining boundary conditions such as contacts and fixed displacements, and assigning specific material parameters to each structure. Such a complete model, called a reference model, is then modified using an image-based nonrigid registration technique to generate patient-specific FE meshes, while preserving mesh topology and boundary conditions.

The main limitation of the method lies in its sensitivity to the presence of artifacts in CT scans. When these artifacts are too important, they alter the voxel values of soft tissues, making it difficult to properly determine the interface between air and soft tissue. These artifacts also make inaccurate the preprocessing of the patient CT scans. When artifacts generate "rays" in the voxels, they can cause the formation of small clusters of pixels (with less than 500 pixels) in the sagittal slices connected to each other in the soft tissue. This occurs particularly in the lip region, which is often affected by the presence of dental appliances. Unfortunately, these clusters of voxels can be mistakenly removed during the preprocessing of the CT scans because they are interpreted as blobs located inside bone structures. Furthermore, as another limitation, although this method is largely automated and can therefore be integrated into a clinical routine, it requires manual intervention by the surgeon (5 min) to position the landmarks on the patients' bone.

In the context of a clinical protocol involving 30 patients (Annecy Hospital, France), future work will enable us to assess quantitatively our capacity to use the thus-designed presurgery patient-specific models in surgery planning by (1) simulating orthognathic bone surgery on patient-specific FE meshes and comparing the corresponding predictions with real data obtained from postoperative CT scans and (2) studying the functionality of muscle structures in patients after surgery. The capacity for our model to predict orofacial functions such as smiling, wincing, or lip rounding for speech is particularly important, since our physically based approach should enable us to go in this respect beyond the performances of approaches based on deep-learning methods [18, 35, 36], which have been shown to be powerful in predicting purely aesthetic aspects.

Acknowledgments

The first author's PhD position is funded by ANSYS France and the French *Agence Nationale de la Recherche Technologique (ANRT)* in the context of a CIFRE contract. Thank you to the participants of the subjective evaluation session of the models for their time. The clinical study was founded by the *Fondation de l'Avenir* (project *Simulation des Parties mOlles faciales en Chirurgie orthognathique (SPOC)*). Open access publication funding provided by COUPERIN CY26.

Funding

The authors have nothing to report.

Ethics Statement

The clinical protocol has been approved by the French Comité de Protection des Personnes (Protocole SPOC, NCT06822127).

Conflicts of Interest

The authors declare no conflicts of interest.

Data Availability Statement

The data that support the findings of this study are available on request from the corresponding author. The data are not publicly available due to privacy or ethical restrictions.

References

1. J. Rustemeyer, A. Groddeck, S. Zwerger, and A. Bremerich, "The Accuracy of Two-Dimensional Planning for Routine Orthognathic Surgery," *British Journal of Oral and Maxillofacial Surgery* 48, no. 4 (2010): 271–275.

2. M. Okudaira, T. Kawamoto, T. Ono, and K. Moriyama, "Soft-Tissue Changes in Association With Anterior Maxillary Osteotomy: A Pilot Study," *Oral and Maxillofacial Surgery* 12 (2008): 131–138.

3. C. U. Joss, I. M. Joss-Vassalli, S. Kiliaridis, and A. M. Kuijpers-Jagtman, "Soft Tissue Profile Changes After Bilateral Sagittal Split Osteotomy for Mandibular Advancement: A Systematic Review," *Journal of Oral and Maxillofacial Surgery* 68, no. 6 (2010): 1260–1269.

4. C. Marchetti, A. Bianchi, L. Muyldermans, M. Di Martino, L. Lancellotti, and A. Sarti, "Validation of New Soft Tissue Software in Orthognathic Surgery Planning," *International Journal of Oral and Maxillofacial Surgery* 40, no. 1 (2011): 26–32.

5. X. Zhang, D. Kim, S. Shen, et al., "An eFTD-VP Framework for Efficiently Generating Patient-Specific Anatomically Detailed Facial Soft Tissue FE Mesh for Craniomaxillofacial Surgery Simulation," *Biomechanics and Modeling in Mechanobiology* 17 (2018): 387–402.

6. D. Kim, T. Kuang, Y. L. Rodrigues, et al., "A Novel Incremental Simulation of Facial Changes Following Orthognathic Surgery Using FEM With Realistic Lip Sliding Effect," *Medical Image Analysis* 72 (2021): 102095.

7. D. Terzopoulos and K. Waters, "Physically-Based Facial Modelling, Analysis, and Animation," *Journal of Visualization and Computer Animation* 1, no. 2 (1990): 73–80.

8. E. Keeve, S. Girod, R. Kikinis, and B. Girod, "Deformable Modeling of Facial Tissue for Craniofacial Surgery Simulation," *Computer Aided Surgery: Official Journal of the International Society for Computer Aided Surgery* 3, no. 5 (1998): 228–238.

9. Y. Zhang, T. Sim, C. L. Tan, and E. Sung, "Anatomy-Based Face Reconstruction for Animation Using Multi-Layer Deformation," *Journal of Visual Languages and Computing* 17, no. 2 (2006): 126–160.

10. W. Mollemans, F. Schutyser, N. Nadjmi, F. Maes, and P. Suetens, "Predicting Soft Tissue Deformations for a Maxillofacial Surgery Planning System: From Computational Strategies to a Complete Clinical Validation," *Medical Image Analysis* 11, no. 3 (2007): 282–301.

11. J. Liebregts, T. Xi, M. Timmermans, et al., "Accuracy of Three-Dimensional Soft Tissue Simulation in Bimaxillary Osteotomies," *Journal of Cranio-Maxillofacial Surgery* 43, no. 3 (2015): 329–335.

20407947, 2026, 2, Downloaded from https://onlinelibrary.wiley.com/doi/10.1002/cnm.70144 by Yohan PAYAN - Cochrane France , Wiley Online Library on [05/02/2026]. See the Terms and Conditions (https://onlinelibrary.wiley.com/terms-and-conditions) on Wiley Online Library for rules of use; OA articles are governed by the applicable Creative Commons License

12. L. Beldie, B. Walker, Y. Lu, S. Richmond, and J. Middleton, "Finite Element Modelling of Maxillofacial Surgery and Facial Expressions – A Preliminary Study," *International Journal of Medical Robotics and Computer Assisted Surgery* 6, no. 4 (2010): 422–430.

13. L. Mf, S. Liao, and T. Rf, "Facial Hexahedral Mesh Transferring by Volumetric Mapping Based on Harmonic Fields," *Computers & Graphics* 35, no. 1 (2011): 92–98.

14. M. Shafi, A. Ayoub, X. Ju, and B. Khambay, "The Accuracy of Three-Dimensional Prediction Planning for the Surgical Correction of Facial Deformities Using Maxilim," *International Journal of Oral and Maxillofacial Surgery* 42, no. 7 (2013): 801–806.

15. C. Resnick, R. Dang, S. Glick, and B. Padwa, "Accuracy of Three-Dimensional Soft Tissue Prediction for Le Fort I Osteotomy Using Dolphin 3D Software: A Pilot Study," *International Journal of Oral and Maxillofacial Surgery* 46, no. 3 (2017): 289–295.

16. P. Knoops, A. Borghi, R. Breakey, et al., "Three-Dimensional Soft Tissue Prediction in Orthognathic Surgery: A Clinical Comparison of Dolphin, ProPlan CMF, and Probabilistic Finite Element Modelling," *International Journal of Oral and Maxillofacial Surgery* 48, no. 4 (2019): 511–518.

17. E. C. Olivetti, S. Nicotera, F. Marcolin, et al., "3D Soft-Tissue Prediction Methodologies for Orthognathic Surgery—A Literature Review," *Applied Sciences* 9, no. 21 (2019): 4550.

18. L. Ma, D. Xiao, D. Kim, et al., "Simulation of Postoperative Facial Appearances via Geometric Deep Learning for Efficient Orthognathic Surgical Planning," *IEEE Transactions on Medical Imaging* 42, no. 2 (2022): 336–345.

19. W. Du, H. Wang, C. Zhao, et al., "Postoperative Facial Prediction for Mandibular Defect Based on Surface Mesh Deformation," *Journal of Stomatology, Oral and Maxillofacial Surgery* 125, no. 5 (2024): 101973.

20. M. Hertanto, A. F. Ayoub, P. C. Benington, K. B. Naudi, and P. S. McKenzie, "Orthognathic Patient Perception of 3D Facial Soft Tissue Prediction Planning," *Journal of Cranio-Maxillofacial Surgery* 49, no. 9 (2021): 783–788.

21. B. Couteau, Y. Payan, and S. Lavallée, "The Mesh-Matching Algorithm: An Automatic 3D Mesh Generator for Finite Element Structures," *Journal of Biomechanics* 33, no. 8 (2000): 1005–1009.

22. M. Chabanas, V. Luboz, and Y. Payan, "Patient Specific Finite Element Model of the Face Soft Tissues for Computer-Assisted Maxillofacial Surgery," *Medical Image Analysis* 7, no. 2 (2003): 131–151.

23. M. Bucki, C. Lobos, and Y. Payan, "A Fast and Robust Patient Specific Finite Element Mesh Registration Technique: Application to 60 Clinical Cases," *Medical Image Analysis* 14, no. 3 (2010): 303–317.

24. A. Bijar, P. Y. Rohan, P. Perrier, and Y. Payan, "Atlas-Based Automatic Generation of Subject-Specific Finite Element Tongue Meshes," *Annals of Biomedical Engineering* 44 (2016): 16–34.

25. I. Stavness, M. A. Nazari, P. Perrier, D. Demolin, and Y. Payan, "A Biomechanical Modeling Study of the Effects of the Orbicularis Oris Muscle and Jaw Posture on Lip Shape," *Journal of Speech, Language, and Hearing Research* 56, no. 3 (2013): 878–890.

26. M. A. Nazari, P. Perrier, M. Chabanas, and Y. Payan, "Simulation of Dynamic Orofacial Movements Using a Constitutive Law Varying With Muscle Activation," *Computer Methods in Biomechanics and Biomedical Engineering* 13, no. 4 (2010): 469–482.

27. M. C. Picard, M. Cotton, N. Briot, et al., "Biomechanical Model of the Human Face With a Perspective of Surgical Assistance," *Computer Methods in Biomechanics and Biomedical Engineering* 26, no. sup1 (2023): S202–S204.

28. J. R. Hutto and S. Vattoth, "A Practical Review of the Muscles of Facial Mimicry With Special Emphasis on the Superficial Musculoaponeurotic System," *American Journal of Roentgenology* 204, no. 1 (2015): W19–W26.

29. M. A. Nazari, P. Perrier, and Y. Payan, "The Distributed Lambda (λ) Model (DLM): A 3-D, Finite-Element Muscle Model Based on Feldman's λ Model; Assessment of Orofacial Gestures," *Journal of Speech, Language, and Hearing Research* 56, no. 6 (2013): 1909–1923.

30. M. A. Nazari, P. Perrier, and Y. Payan, "Interwoven Muscle Fibers: A 3D Two-Fiber Muscle Active Model. *47th Congress of the Society of Biomechanics*," *Computer Methods in Biomechanics and Biomedical Engineering* 25, no. sup1 (2022): S226–S228.

31. G. G. Barbarino, M. Jabareen, and E. Mazza, "Experimental and Numerical Study on the Mechanical Behavior of the Superficial Layers of the Face," *Skin Research and Technology* 17, no. 4 (2011): 434–444.

32. S. Klein, M. Staring, K. Murphy, M. A. Viergever, and J. P. Pluim, "Elastix: A Toolbox for Intensity-Based Medical Image Registration," *IEEE Transactions on Medical Imaging* 29, no. 1 (2009): 196–205.

33. C. Fouard, A. Deram, Y. Keraval, and E. Promayon, "CamiTK: A Modular Framework Integrating Visualization, Image Processing and Biomechanical Modeling," in *Soft Tissue Biomechanical Modeling for Computer Assisted Surgery* (Springer Berlin Heidelberg, 2012), 323–354.

34. W. E. Lorensen and H. E. Cline, "Marching Cubes: A High Resolution 3D Surface Construction Algorithm," in *Seminal Graphics: Pioneering Efforts That Shaped the Field* (Association for Computing Machinery, 1998), 347–353.

35. N. Lampen, D. Kim, X. Fang, et al., "Deep Learning for Biomechanical Modeling of Facial Tissue Deformation in Orthognathic Surgical Planning," *International Journal of Computer Assisted Radiology and Surgery* 17, no. 5 (2022): 945–952.

36. X. Fang, D. Kim, X. Xu, et al., "Deep Learning-Based Facial Appearance Simulation Driven by Surgically Planned Craniomaxillofacial Bony Movement," in *International Conference on Medical Image Computing and Computer-Assisted Intervention* (Springer Nature Switzerland, 2022), 565–574.

20407947, 2026, 2, Downloaded from https://onlinelibrary.wiley.com/doi/10.1002/cnm.70144 by Yohan PAYAN - Cochrane France , Wiley Online Library on [05/02/2026]. See the Terms and Conditions (https://onlinelibrary.wiley.com/terms-and-conditions) on Wiley Online Library for rules of use; OA articles are governed by the applicable Creative Commons License